the bubble's bottom. The primary wake seems to be closed and not turbulent. This could not be completely determined because of the lack of resolution in the measurements. The primary wake length for trajectories close to the wall is extended to a distance of 3 $d_b$. However, it was distorted and of smaller volume than that of the case of bubble trajectory along the pipe core. It was not possible to determine whether the wake is closed or open. The flow barrier was also generated but was restricted to an area of the bubble size.

Recent experimental investigations (Lunde & Perkins 1997; Brücker 1999) have shown that for spiraling bubbles two parallel counter-rotating vortex filaments are attached to the bubble's rear. The wake of zigzagging (moving only in a plane) and rocking (non-coplanar motion) bubbles, instead, is intermittent, and consists of hairpin vortices. These are shed from the bubble surface with more or less regular frequency, although the vortex shape depends on the bubble size. These results are applicable, however, only to situations where wall influence is negligible. As mentioned before, the rocking and spiraling bubble motion was predominant in this experiment. Therefore, a combination of continuous trailing wake and vortex shedding is expected. However, due to the averaging process, in which the bubble rocking motion was not considered, the wake structure cannot be completely described. The results obtained here seem to indicate the wake structure associated with a spiraling bubble, more than a rocking one, at least for the primary wake. For the far wake, it seems more probable that the irregular vortex structures observed are originated from vortex shedding, and then associated to rocking bubble motion. The vortex structures shed from the bubble's surface do not spread because of the wall. Further, the constant interaction of these vortex spots with the wall, between themselves, and with the mean and turbulent flow, distorted the circulatory motion.

### *5.5. Turbulent flow field description*

It should be noted that the spatial resolution of the present measurements close to the bubble's thin boundary layer is not enough to resolve the large velocity gradient close to the bubble surface. The location of the high turbulence spots was studied in detail to determine their behavior with regards to the mean flow. It was noted that the turbulence spots are usually at the same distance from the bubble. Therefore, such turbulence spots are being continuously generated as the bubble rises up. However, the turbulent kinetic energy is not always the same at such spots. Figures 29 to 32 show the distribution of the turbulent kinetic energy at $t_p$ = 33.33 ms, for the two bubble trajectories studied here. It can be deduced from the figures that when the

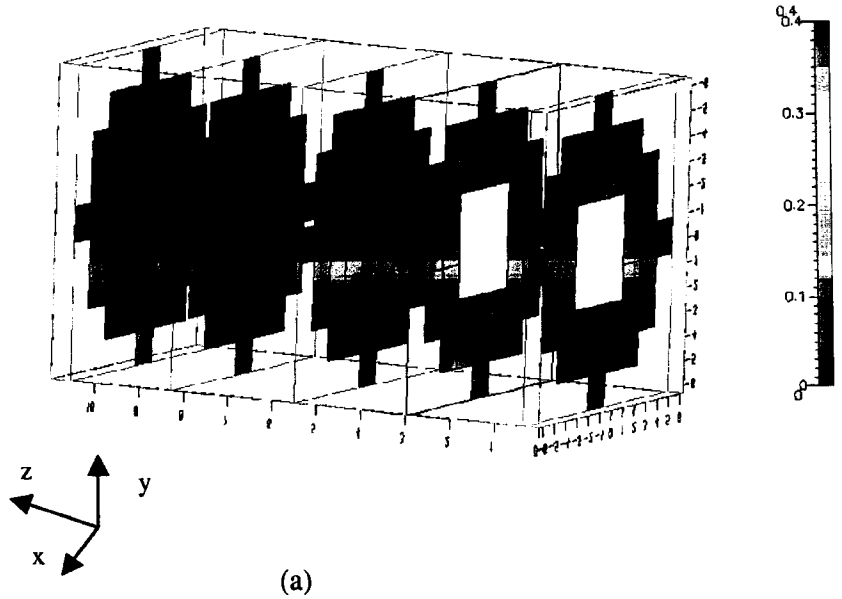


(a)

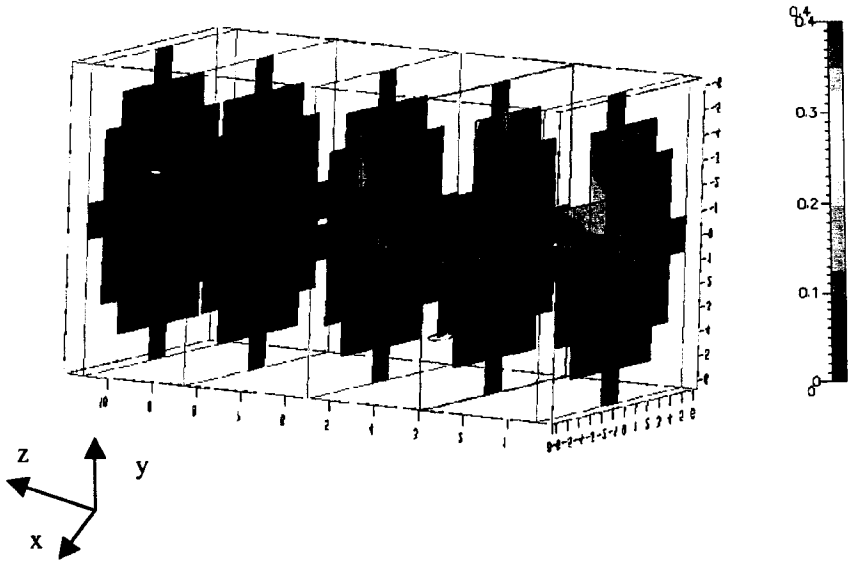


(b)

Figure 29. Distribution of turbulent kinetic energy, in μJ, at $t_p$ = 0 ms. a) Bubble trajectory along the pipe center; and b) bubble trajectory close to the pipe wall.

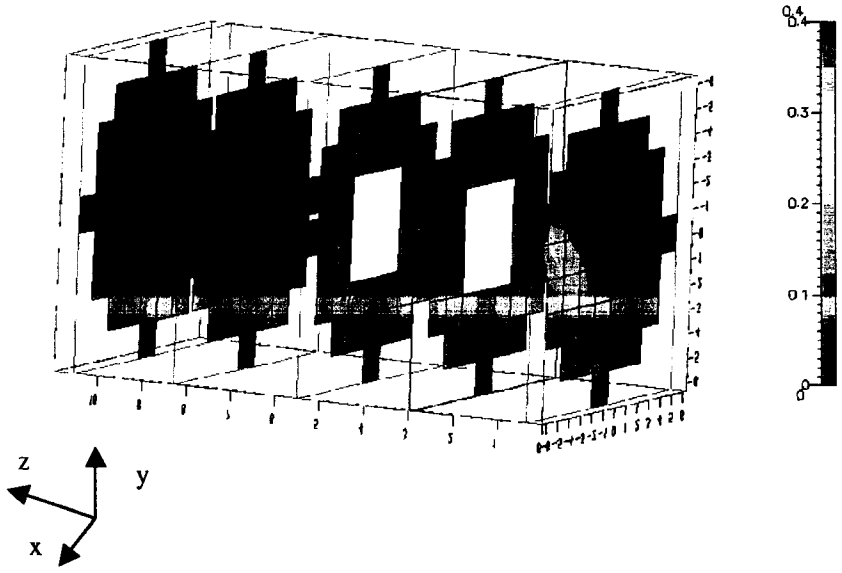


(a)

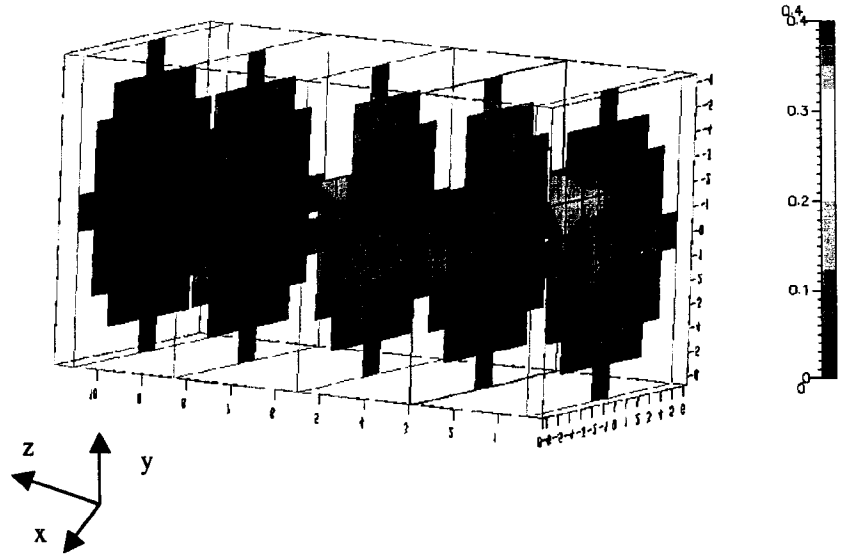


(b)

Figure 30. Distribution of turbulent kinetic energy, in μJ, at $t_p$ = 16.67 ms. a) Bubble trajectory along the pipe center; and b) bubble trajectory close to the pipe wall.

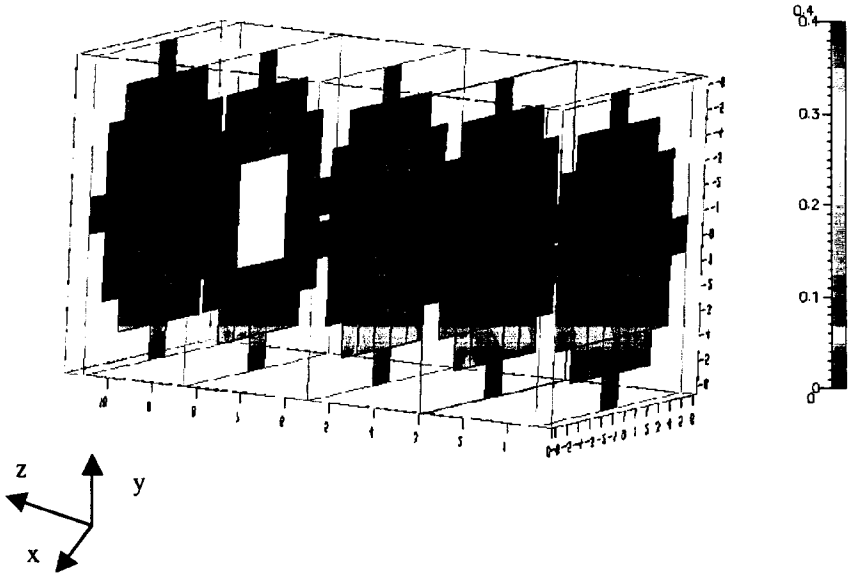


(a)

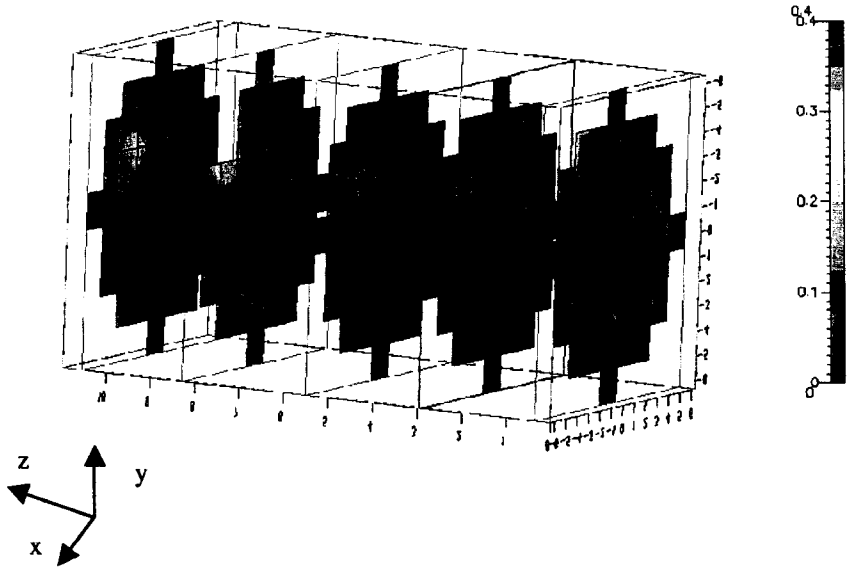


(b)

Figure 31. Distribution of turbulent kinetic energy, in μJ, at $t_p$ = 33.33 ms. a) Bubble trajectory along the pipe center; and b) bubble trajectory close to the pipe wall.

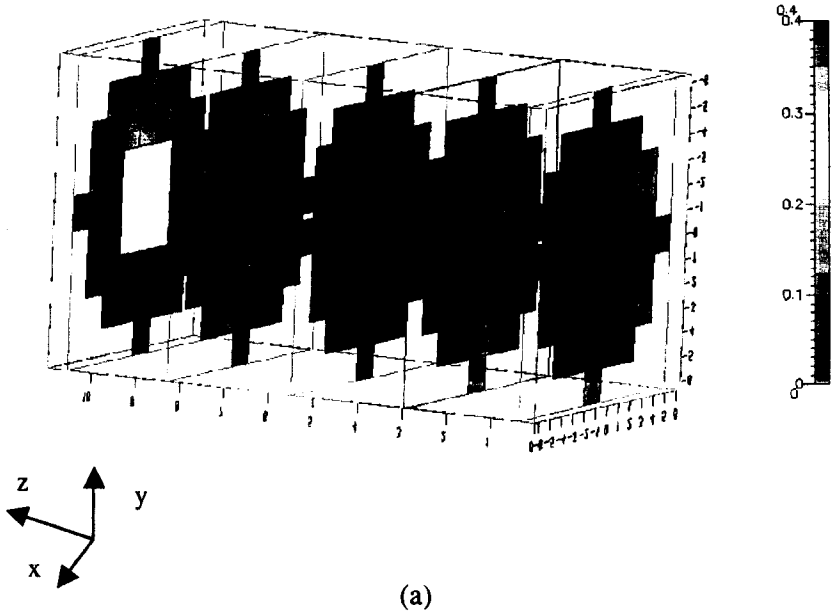


(a)

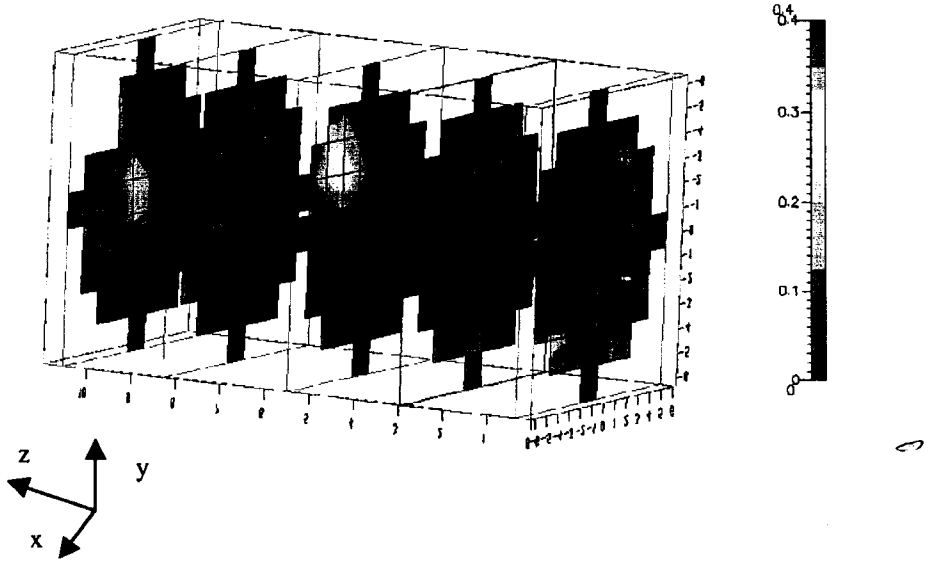


(b)

Figure 32. Distribution of turbulent kinetic energy, in μJ, at $t_p$ = 50.0 ms. a) Bubble trajectory along the pipe center; and b) bubble trajectory close to the pipe wall.

bubble travels close to the pipe wall, it generates more turbulence than for the case when the bubble trajectory is along the center of the pipe. Plots for the turbulence intensities and Reynolds stresses are shown in figures 33 to 38. These plots are for trajectories along the pipe core and close to the pipe wall, at $t_p = 33.33$ ms.

The turbulent intensities $\sqrt{\overline{u'^2}}$ and $\sqrt{\overline{w'^2}}$ are extended farther upstream, when the bubble is rising close to the wall. For the case of $\sqrt{\overline{v'^2}}$, it reaches about the same distance for both bubble trajectories. The presence of the turbulent intensities, downstream of the rising bubble, is farther when bubble trajectory is close to the wall. The magnitudes of $\sqrt{\overline{u'^2}}$ and $\sqrt{\overline{w'^2}}$ are higher for bubble trajectory close to the pipe wall; but the opposite happens in the pipe core for $\sqrt{\overline{v'^2}}$. These results are in agreement with the characteristics of the flow.

*5.6. Transient analysis of the kinetic energy*

Figure 39 shows the behavior of the mean, turbulent and total kinetic energy through the whole measurement, for both bubble trajectory cases studied here. In this figure, time step 0 corresponds to the first frame in which the bubble is present in the viewing volume. Observe that on the moments in which the bubble is present in the test zone, the mean kinetic energy in the volume, and consequently the total kinetic energy, reaches its maximum. The sharp increase and decrease of energy in the volume are observed at the first frame (time $t_p = 0$ ms) in which the bubble is the test zone, and the second frame after the bubble has departed the viewing volume (time $t_a = 16.67$ ms), respectively. It can also be seen in figure 39 that the mean kinetic energy is higher when the bubble rises along the center of the pipe. This is because practically all the flow is accelerated due to reduced flow area available. In the case of the bubble close to the pipe wall, the flow away from the bubble does not reach the same high acceleration as in the case of the bubble rising along the pipe center, as explained above.

With respect to the turbulent kinetic energy, once the bubble and its primary wake have left the test zone, the close-to-the-wall bubble trajectories generate more turbulence. This could be explained by considering vortex shedding. It is known that vortex shedding is reduced, and even suppressed, when the distance between a bluff object and the container wall is small (Bosch *et al.* 1996). Since the vortex shedding may not be periodic in this case (due to the combination of rocking and spiraling bubble motion), and the vortex strength could be lower, the surrounding

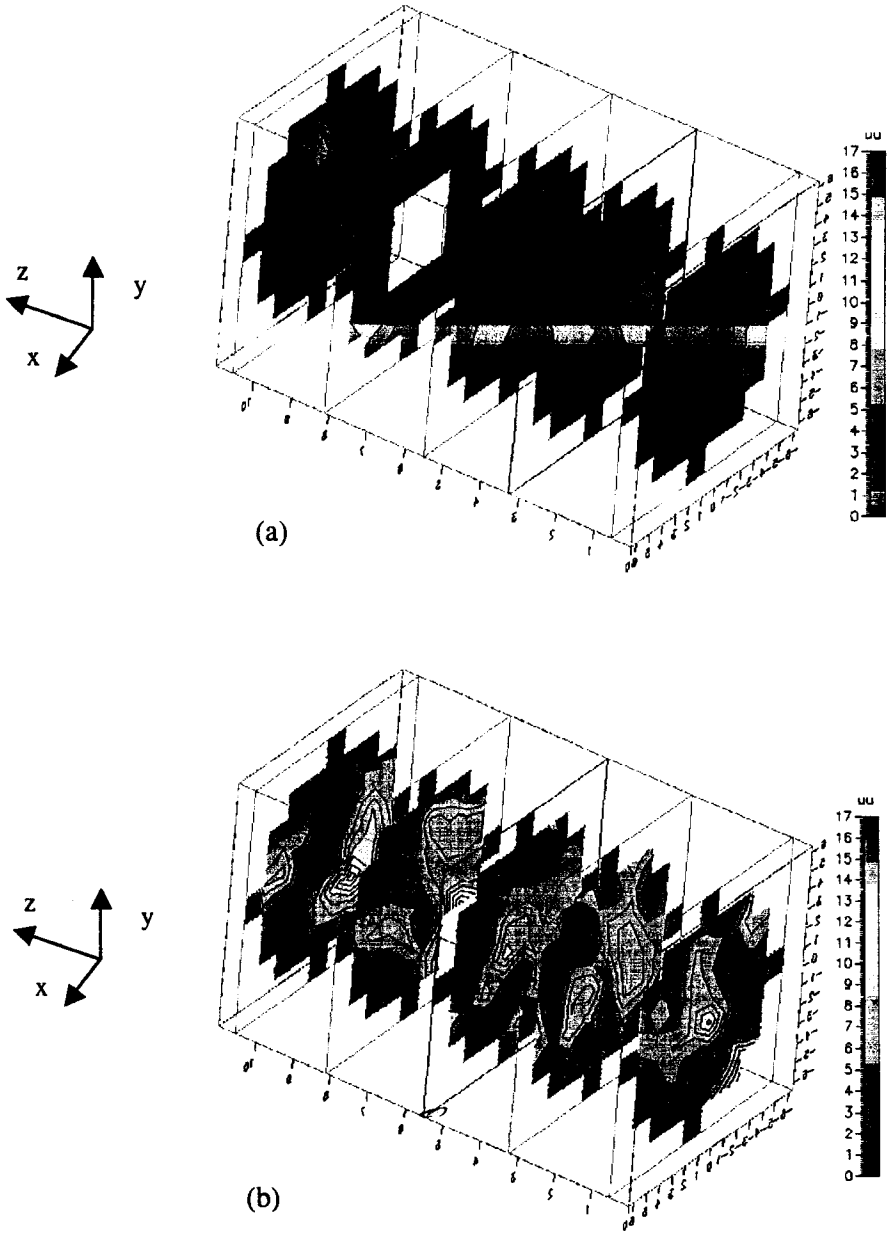


Figure 33. Turbulence intensity $\sqrt{\overline{u'u'}}$ in mm/s. The data presented are for $t_p$ = 33.33 ms after the bubble enters the viewing volume. (a) Bubble trajectory along the pipe core; and (b) bubble close to the pipe wall.

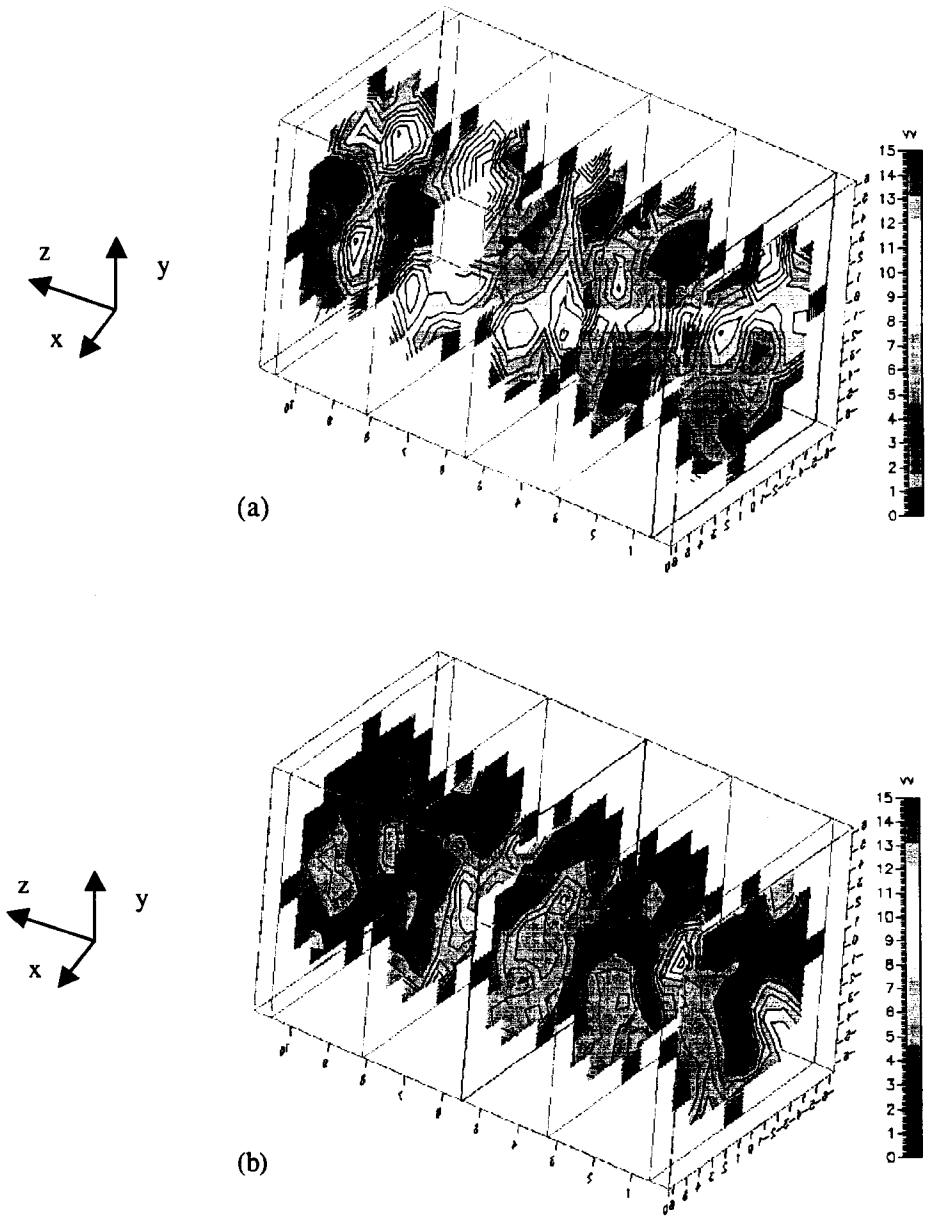


Figure 34. Turbulence intensity $\sqrt{\overline{v'v'}}$ in mm/s. The data presented are for $t_p$ = 33.33 ms after the bubble enters the viewing volume. (a) Bubble trajectory along the pipe core; and (b) bubble close to the pipe wall.

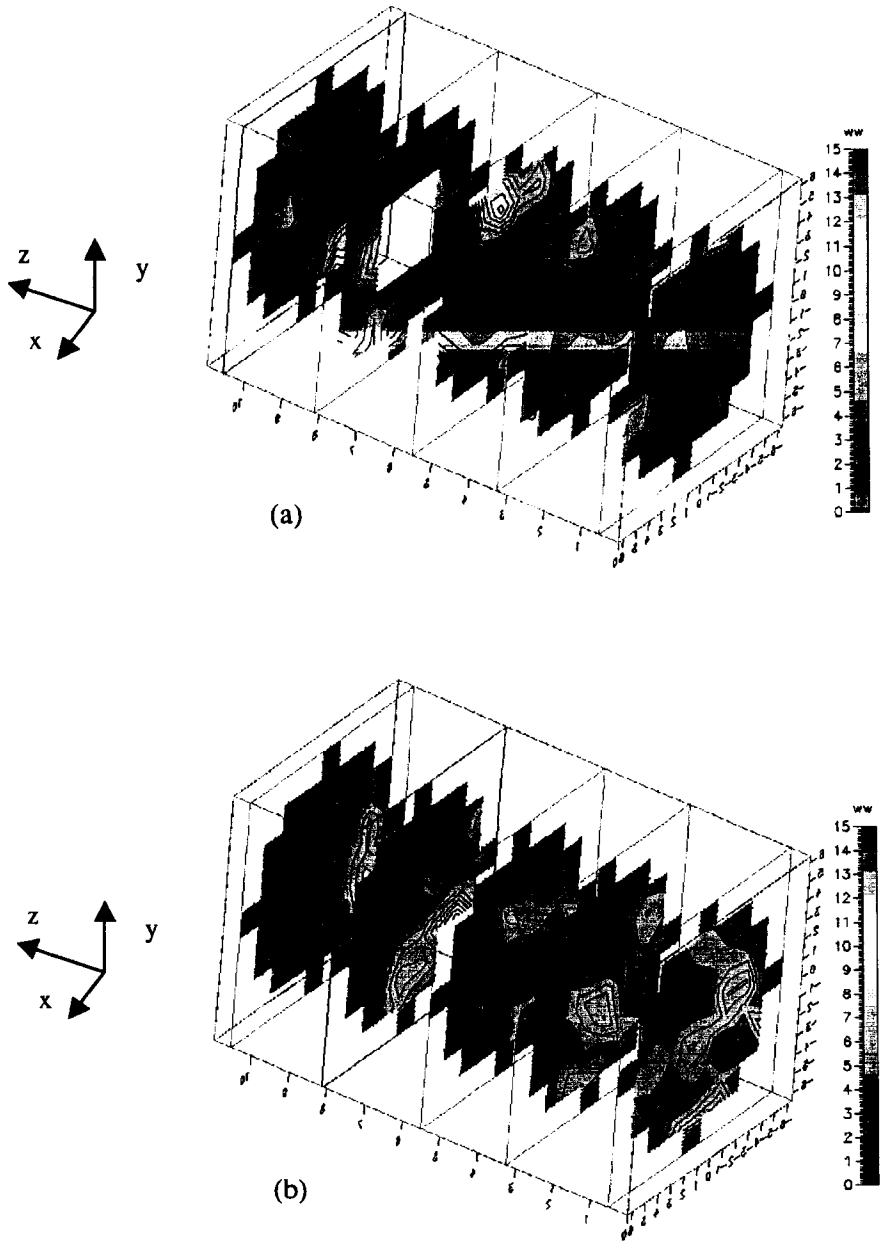


Figure 35. Turbulence intensity $\sqrt{\overline{w'w'}}$ in mm/s. The data presented are for $t_p$ = 33.33 ms after the bubble enters the viewing volume. (a) Bubble trajectory along the pipe core; and (b) bubble close to the pipe wall.

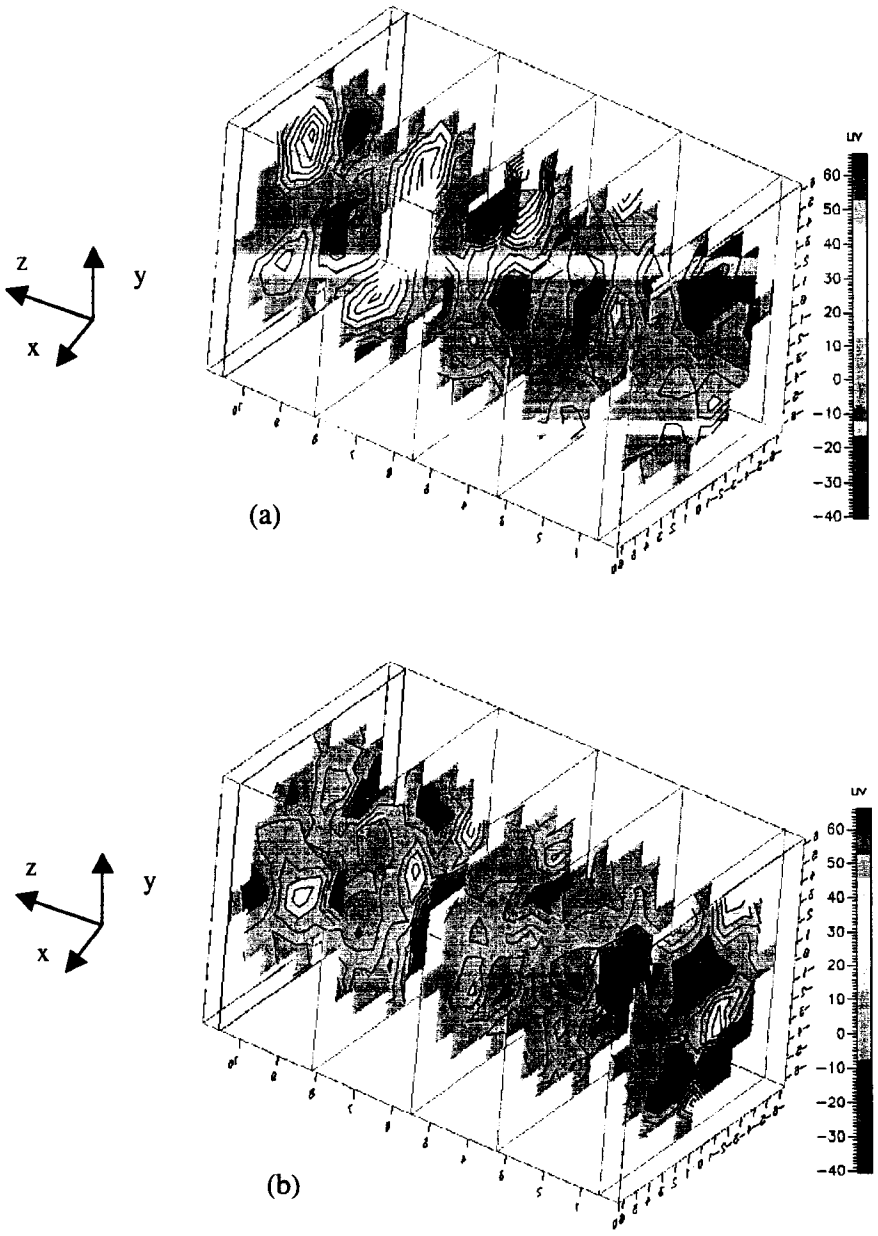


Figure 36. Reynolds stresses $\overline{u'v'}$ in $mm^2/s^2$. The data presented are for $t_p$ = 33.33 ms after the bubble enters the viewing volume. (a) Bubble trajectory along the pipe core; and (b) bubble close to the pipe wall.

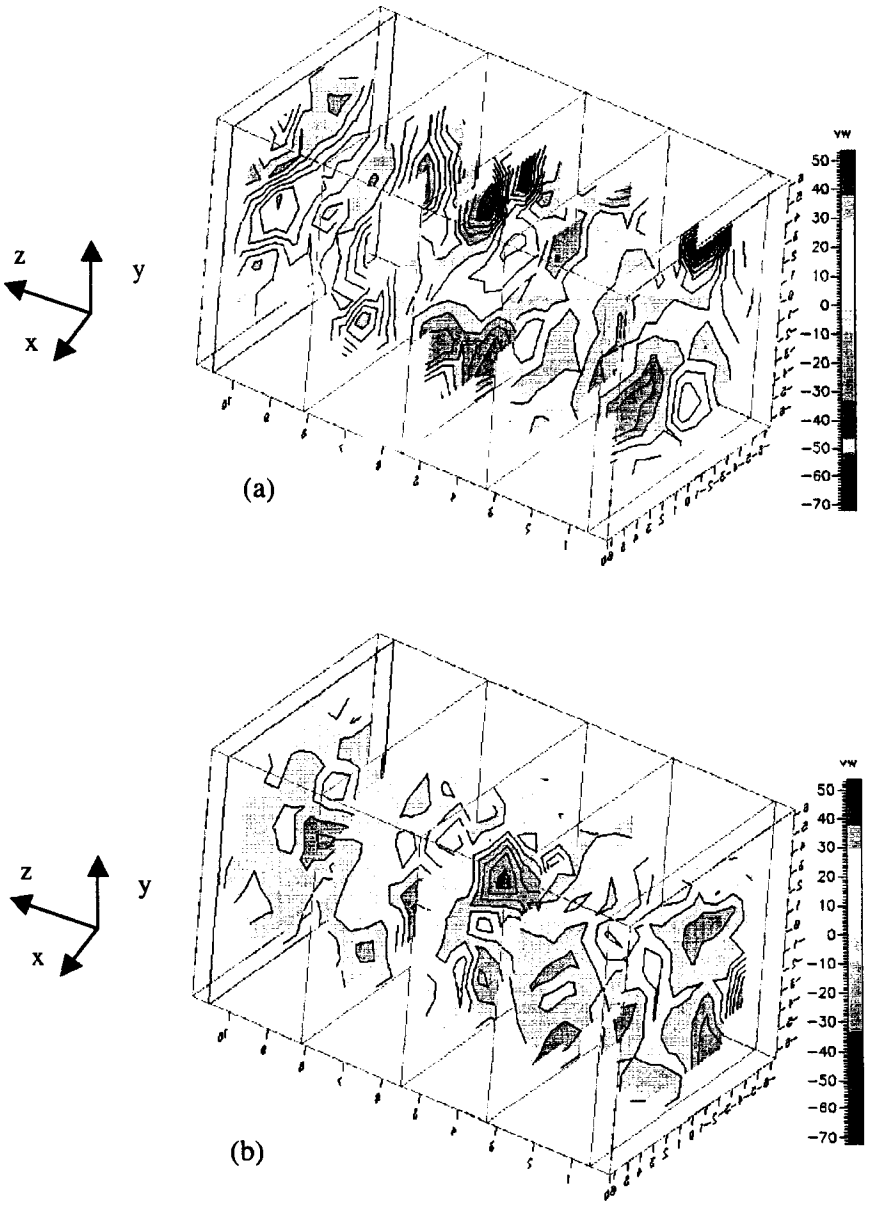


Figure 37. Reynolds stresses $\overline{v'w'}$ in $mm^2/s^2$. The data presented are for $t_p$ = 33.33 ms after the bubble enters the viewing volume. (a) Bubble trajectory along the pipe core; and (b) bubble close to the pipe wall.

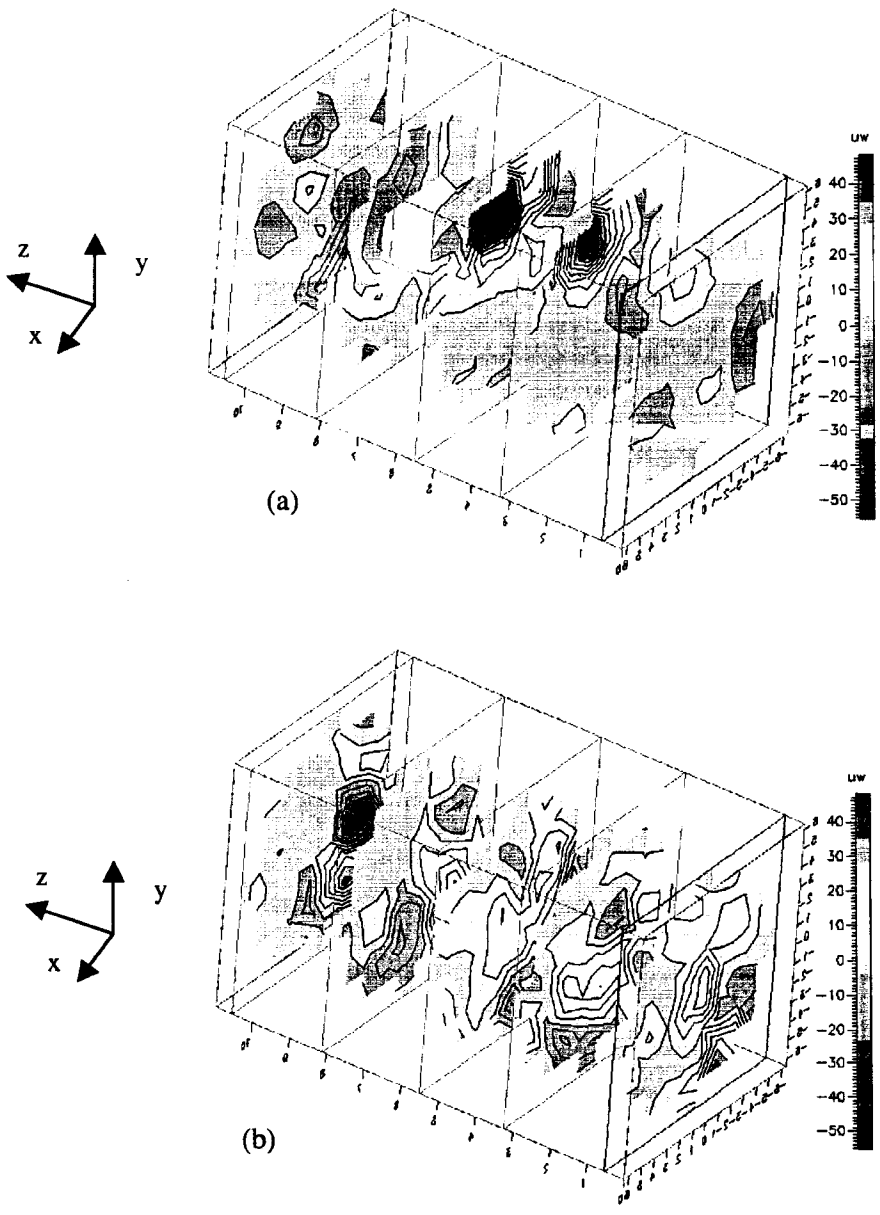


Figure 38. Reynolds stresses $\overline{u'w'}$ in $mm^2/s^2$. The data presented are for $t_p$ = 33.33 ms after the bubble enters the viewing volume. (a) Bubble trajectory along the pipe core; and (b) bubble close to the pipe wall.

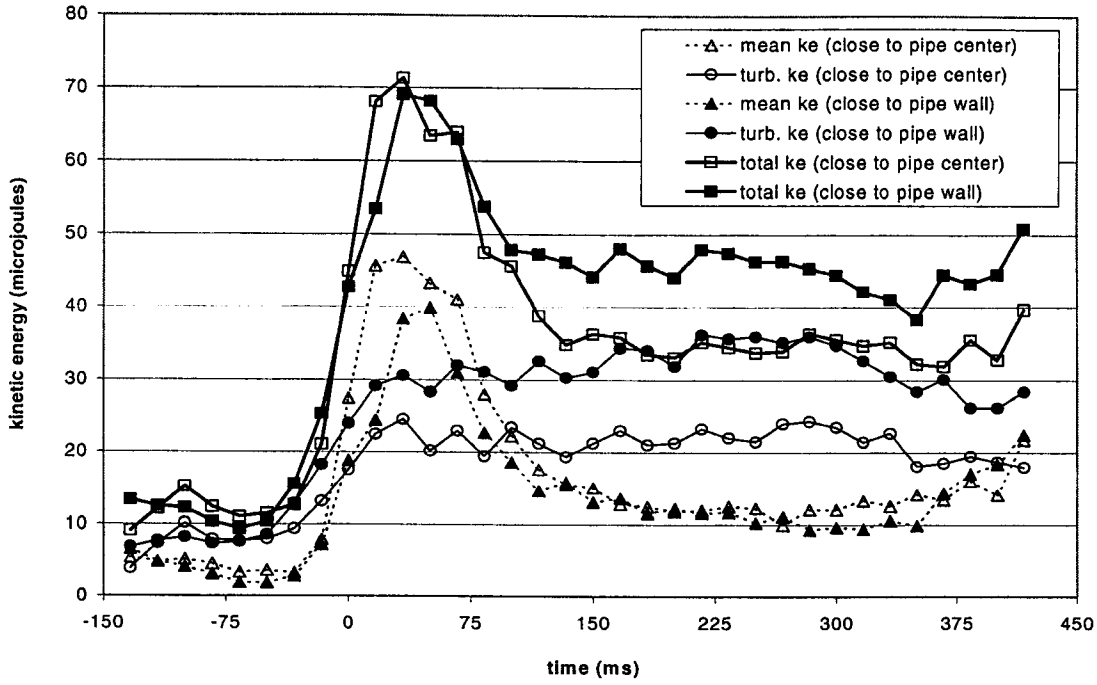


Figure 39. Transient behavior of the kinetic energy in the test volume. Time 0 corresponds to when the bubble is first present in the viewing volume.

turbulent flow in the wake can easily distort the vortex pattern. This indicates that the bubble's wake is turbulent for such trajectories close to the wall. In the case of the bubble rising along the center of the pipe, the vortex shedding from the bubble's surface is more periodic, that in the case when the bubble rocks. Thus, the turbulence generated in both cases is due to interaction between flow, which after colliding with the wall is redirected towards the pipe center, and the vortex structures arriving into the volume.

It is important to note that the total kinetic energy is practically the same when the bubble is in the viewing volume for both bubble trajectories. The maximum is reached at the third time step the bubble is present in the test zone ($t_p$ = 33.33 ms). This maximum is about 70.0 μJ. The results indicate that bubbles of similar size bring the similar amount of momentum into the test volume. To get a better idea of how much energy is brought by the bubble in the test volume, consider the velocity magnitude corresponding to 70.0 μJ. The speed of the liquid in the test volume would be about 33.0 cm/s. This is about 50% higher than the speed of the bubble alone.

It is also interesting to note that the decay of the kinetic energy is practically the same for both trajectories. The difference exists because more turbulence is generated by the bubbles rising close to the wall, as explained before. After the primary wake completely leaves the measurement zone ($t_a$ = 33.33 ms), the transient behavior of the total kinetic energy is practically constant. This indicates that the decay constant is more than 4.0 μJ/s.

The previous results allow for deducing some important conclusions about the use of potential flow theory in the description of the flow around a bubble and within its wake when wall influence is important. Potential flow can only be applied for regions two $d_b$ downstream of the bubble, when the bubble rises along the center of the pipe. For the case of a bubble rising close to the wall, potential flow can be used three $d_b$ downstream, and at least one $d_b$ away of the bubble surface in the radial direction. Within the bubble's wake, several small zones of high vorticity and turbulence were observed during all the time steps after the bubble left the viewing volume. Therefore, potential flow theory should not be considered to describe the flow within the wake of a bubble, especially when wall influence is important.

# CHAPTER VI
# SHAPE, TRAJECTORY AND FORCES ACTING ON A BUBBLE RISING IN A SMALL DIAMETER PIPE

Bubble characteristics are of considerable importance in determining performance in various two-phase flows, for example in gas absorption, chemical reactors, and boiling heat transfer. The bubble dynamic results are useful in extending the knowledge of bubble behavior in two-phase systems and in providing data to test flow models and correlations. A bubble shape cannot be completely predicted unless all the physical variables pertinent to the bubble rise phenomenon are taken into account. Shape and trajectory of a bubble moving in a liquid are the consequence of the forces acting on it, and the surrounding flow field. The motion of bubbles rising in stagnant water has been experimentally studied extensively since the 50's. In most cases, wall influence was not considered in the results. The study of the motion of bubbles in restricted containers has focused on the measurements of terminal velocities and steady drag coefficients. In the last decade, numerical simulations have been performed to compute the trajectories of particles in non-uniform and unsteady flows, although the models used are very restrictive in most cases. The theoretical analysis mainly concern with the accurate description of the forces acting on the bubble, and how to include them in the motion equation.

In this chapter, the results concerning the shape, trajectory and drag and lift forces for an ellipsoidal bubble rising in quiescent water, in a small diameter pipe, are presented, compared against known results in the literature, and discussed.

## *6.1. Theoretical background*

When an air bubble is released in water, it will rise up due to buoyancy only, if no other external forces exist on the system. Depending on the bubble dimensions, it will attain a determined shape and trajectory. It is commonly accepted that bubbles of less than about 1 mm of equivalent diameter are spherical and have a linear rising trajectory. Bubbles larger than 6 mm of equivalent diameter follow a straight path too, but their shape is close to a spherical-cap. In the range in between, 2 and 6 mm, bubbles are ellipsoidal. They are not necessarily symmetric, or wobble. The trajectory can be a zigzag, spiral, and/or a combination of those two paths.

Rocking motion is frequently observed.

*6.1.1. Bubble shape*

Bubble shape information, although still somewhat qualitative, is presented graphically in terms of three dimensionless groups: the Reynolds number, the Eötvös number, and the Morton number (Grace 1973; Bhaga & Weber 1981). The Eötvös number, Eo, is given by

$$\mathrm{Eo} = \frac{g\,\Delta\rho\,d_e^2}{\sigma}, \qquad [43]$$

where $g$ is the magnitude of the gravity vector, $\Delta\rho$ is the difference between the bubble's medium density and liquid fluid density, $d_e$ is the spherical equivalent diameter of the bubble, and $\sigma$ is the surface tension of the liquid fluid. The Morton number, M, is given by

$$\mathrm{M} = \frac{g\,\mu^4\Delta\rho}{\rho^2\sigma^3}, \qquad [44]$$

where the liquid fluid has viscosity $\mu$, and density $\rho$.

Most of the experimental and numerical studies of single bubble dynamics are performed with the assumption that the container walls have negligible influence on the behavior of the bubble. According to Clift *et al.* (1978) for wall effect $\lambda \leq 0.6$ ($\lambda = d_e / D$, where $D$ is the pipe diameter) and Eo < 40, some empirical correction factors, depending on the bubble's Reynolds number, $\mathrm{Re}_b$, and $\lambda$ can be used for predictions of terminal velocities and drag coefficients. The bubble Reynolds number, $\mathrm{Re}_b$, is given by

$$\mathrm{Re}_b = \frac{U_b\,d_e}{\nu}, \qquad [45]$$

where $\nu$ is the kinematic viscosity of the liquid. Regarding the bubble shape, for intermediate $\mathrm{Re}_b$, the observation indicated that bubbles tend to be flat in the perpendicular direction of motion, and the wall tends to elongate the bubble along the flow direction. Therefore, the final

resultant shape would be close to a spheroid. The change in shape, however, induces changes in the shedding frequency, and consequently, the complexity of the flow structure increases.

Among the numerical studies of bubble shapes and trajectories, Tomiyama (1998) considered bubble motion and shape in stagnant liquid as a function of M and Eo numbers. In his 3D simulation, an agreement with Grace's graphical correlation for the bubble shape was obtained. The bubble trajectory was studied in two dimensions only. The results showed that for a given M, an increase in Eo leads the bubble to follow a zigzag path, with a change in the shape from spheroidal to wobbling. This behavior is also confirmed by Grace *et al.* (1976).

*6.1.2. The equation of motion*

The trajectory of a particle is computed by integrating the momentum, or motion equation. A recent review of the equation of motion for particles, bubbles, and droplets has been presented by Michaelides (1997). The equation of motion of a particle moving in a uniform fluid can be written as (Magnaudet 1997)

$$m_p \frac{d\mathbf{v}}{dt} = m_p \mathbf{g} + m_f \left( \frac{D\mathbf{u}}{Dt} - \mathbf{g} \right) + \mathbf{F}_p , \qquad [46]$$

where the subscripts $p$ and $f$ refer to the particle and fluid, respectively, $m$ is the mass, $\mathbf{g}$ is the gravity vector, $\mathbf{u}$ is the velocity of the fluid in the absence of the particle (the undisturbed velocity), $\mathbf{v}$ is the velocity of the particle, and $\mathbf{F}_p$ are all the hydrodynamic forces resulting from the presence of the particle in the flow. The second term in the right hand side is the force exerted by the flow on the volume of fluid occupied by the particle. The substantial derivatives for both the particle and the fluid are given by [34]. When the velocity $\mathbf{u}$ is non-uniform, the so-called Faxen force needs to be included into [46]. This force is proportional to $\nabla^2 \mathbf{u}$.

The contributions to the total hydrodynamic force $\mathbf{F}_p$ come from the drag force $\mathbf{F}_D$, the lift force $\mathbf{F}_L$, the added-mass (virtual mass) force $\mathbf{F}_M$, and the Basset or history force, $\mathbf{F}_B$, that is

$$\mathbf{F}_p = \mathbf{F}_D + \mathbf{F}_L + \mathbf{F}_M + \mathbf{F}_B . \qquad [47]$$

$\mathbf{F}_B$ is significant for very small Re. Domgin *et al.* (1998) showed that $\mathbf{F}_B$ is only 1.4% of the